Supporting Information

Site-Specific Fluorination on Donor–Acceptor Polymers Enhances Intramolecular Charge Transfer for Photocatalytic Hydrogen Evolution

Wooteak Jung,[a, †] Sanghyeok An,[a, †] Gayoung Ham,[b, †] Geoneop Choi,[a] Soyeon Lee,[c] Kyo Bin Park,[a] Jiwoong Yang,[c,d] Dae Sung Chung,[a,] and Hyojung Cha[b,*]*

[a.] *Department of Chemical Engineering, Pohang University of Science and Technology (POSTECH), Pohang, 37673, Republic of Korea*

[b.] *School of Energy Engineering, Kyungpook National University, 80 Daehak-ro, Buk-gu, Daegu, 41566, Republic of Korea.*

[c.] *Department of Energy Science and Engineering, Daegu Gyeongbuk Institute of Science and Technology (DGIST), Daegu 42988, Republic of Korea*

[d.] *Energy Science and Engineering Research Center, Daegu Gyeongbuk Institute of Science and Technology (DGIST), Daegu 42988, Republic of Korea*

† *Wooteak Jung, Sanghyeok An and Gayoung Ham contributed equally to this work*

Contents

(d–f) Diiodomethane contact angles of PBF8BT, PBF8BT-AF, and PBF8BT-DF, recorded as 44.72°, 47.75°, and 44.52°, respectively. The corresponding surface energies derived from the water contact angles were 48.09, 44.21, and 46.44 mN m^{-1} for PBF8BT, PBF8BT-AF, and PBF8BT-DF, respectively. The surface energy of polymer thin films was calculated using the Owens–Wendt–Rabel–Kaelble (OWRK) method.

Figure S11. Time-resolved photoluminescence (TR-PL) decay profiles of PBF8BT and PBF8BT-AF Pdots measured by time-correlated single photon counting (TCSPC). (a, c) TR-PL decays of PBF8BT Pdots monitored at 700 and 650 nm, respectively, under three conditions: without Pt cocatalyst, with Pt cocatalyst, and with Pt cocatalyst plus ascorbic acid (AA). (b, d) Corresponding TR-PL decays of PBF8BT-AF Pdots under the same conditions.

Figure S12. Transient absorption kinetics of nanoparticles based on PBF8BT (green), PBF8BT-DF (blue), and PBF8BT-AF (red) probed at (a) 470 nm, (b) 580 nm, and (c) 720 nm.

Figure S13. Transient absorption spectroscopy of nanoparticles under photocatalytic conditions. TAS spectra of (a-b) PBF8BT and (c-d) PBF8BT-DF measured in the absence (left) and presence (right) of ascorbic acid (AA) and Pt cocatalyst. TAS kinetics of PBF8BT-DF at probe wavelengths of (e) 470 nm and (f) 600 nm, comparing the relaxation behaviors with and without AA and Pt.

Table S1. Thermal, optical, and electrochemical properties of the PBF8BT.

Table S2. Summary of residual palladium (Pd) in synthesized polymers, PBF8BT, PBF8BT-AF, and PBF8BT-DF, respectively.

Table S3. Time-resolved photoluminescence (TR-PL) decay lifetime of PBF8BT series excited at 450 nm and probed at 680 nm. The decay kinetics were fitted using a bi-exponential function: $I(t) = A_1 \exp(-t/\tau_1) + A_2 \exp(-t/\tau_2)$.

Table S4. TR-PL decay lifetime of PBF8BT-DF with various conditions, without Pt, with Pt, or with AA and Pt excited at 450 nm and probed at 700 nm. The decay kinetics were fitted using a bi-exponential function: $I(t) = A_1 \exp(-t/\tau_1) + A_2 \exp(-t/\tau_2)$.

Table S5. Kinetic parameters derived from the ns-TA decay kinetics of fluorinated polymer Pdots (PBF8BT-AF and PBF8BT-DF). Comparison of the decay lifetimes (τ_1 and τ_2) and their corresponding amplitudes (A_1 and A_2) at 470 nm and 580 nm. The decay kinetics were fitted using a bi-exponential function: $I(t) = A_1 \exp(-t/\tau_1) + A_2 \exp(-t/\tau_2)$.

Table S6. Kinetic parameters derived from the ns-TA decay kinetics of fluorinated polymer Pdots (PBF8BT, PBF8BT-AF and PBF8BT-DF). Comparison of the decay lifetimes (τ_1 and τ_2) and their corresponding amplitudes (A_1 and A_2) at 720 nm. The decay kinetics were fitted using a bi-exponential function: $I(t) = A_1 \exp(-t/\tau_1) + A_2 \exp(-t/\tau_2)$.

Table S7. Bi-exponential fitting parameters extracted from transient absorption (TA) decay kinetics of PBF8BT-DF monitored at 470 and 600 nm under operative conditions (with Pt cocatalyst and ascorbic acid (AA)). Comparison of the decay lifetimes (τ_1 and τ_2) and their corresponding amplitudes (A_1 and A_2). The decay kinetics were fitted using a bi-exponential function: $I(t) = A_1 \exp(-t/\tau_1) + A_2 \exp(-t/\tau_2)$.

1. Materials and synthesis

Materials: All commercially available reagents and solvents were directly used without further purification. 2,6-bis(trimethytin)-4,8-bis(5-(2-ethylhexyl)-4-fluorothiophen-2-yl)benzo[1,2-b:4,5-b']dithiophene (BDTT-FS-n), (4,8-bis(5-(2-ethylhexyl)thiophen-2-yl)benzo[1,2-b:4,5-b']dithiophene-2,6-diyl)bis(trimethylstannane) (BDTT-Sn), 2,2'-(9,9-dioctyl-9H-fluorene-2,7-diyl)bis(4,4,5,5-tetramethyl-1,3,2-dioxaborolane), 4,7-Dibromo-2,1,3-benzothiadiazole, and 4,7-Dibromo-5,6-difluoro-2,1,3-benzothiadiazole were purchased from Ossila. Tri(o-tolyl)phosphine ($P(o\text{-}tol)_3$, 97%), Potassium phosphate tribasic (K_3PO_4, 98%), Tris(dibenzylideneacetone)dipalladium(0), ($Pd_2(dba)_3$, 97%) were purchased from Sigma Aldrich.. The synthetic procedure is described below.

Synthesis of PBF8BT-AF*:* Pure product of 2,2'-(9,9-dioctyl-9H-fluorene-2,7-diyl)bis(4,4,5,5-tetramethyl-1,3,2-dioxaborolane) (146.06 mg, 0.75 eq, 0.227 mmol), 4-7-dibromo-5-6-difluoro-2-1-3-benzothiadiazole (100 mg, 1 eq, 340 mmol), BDTT-Sn (68.54mg, 0.25 eq, 0.085 mmol) , $Pd_2(dba)_3$ (13.88 mg, 0.05 eq, 0.015 mmol), and $P(o\text{-}tol)_3$ (13.88 mg, 0.15 eq, 0.045 mmol), K_3PO_4 (257.34 mg, 4.0 eq, 1.21 mmol) in 5 mL anhydrous toluene and stirred in 105°C for 5 hours and 1 mL degassed DI was added. Polymerized using thermal reactor (reaction condition: 105 °C 7 days) under Ar. Then, the polymer was end cap using and bromobenzene and phenylboronic acid. Polymer mixture was cooled to room temperature, and the viscous mixture was poured into methanol (≈ 400 mL). After stirring for 1h, the precipitated solid was collected by gravity filtration. The crude polymer solid was subjected to sequential Soxhlet extractions with methanol, acetone, hexane, and chloroform. Finally, the concentrated chloroform solution (≈ 1 mL) was precipitated into methanol (≈ 200 mL). The final precipitate was collected by vacuum filtration and dried under reduced pressure to give the pure polymer as an brown solid .

Synthesis of PBF8BT-DF*:* Pure product of 2,2'-(9,9-dioctyl-9H-fluorene-2,7-diyl)bis(4,4,5,5-tetramethyl-1,3,2-dioxaborolane) (163.94 mg, 0.75 eq, 255 mmol), 4,7-dibromobenzo[c][1,2,5]thiadiazole (100 mg, 1 eq, 340 mmol), BDTT-F-Sn (79.98 mg, 0.25 eq, 0.085 mmol) , $Pd_2(dba)_3$ (15.58 mg, 0.05 eq, 0.017 mmol), and $P(o\text{-}tol)_3$ (15.57 mg, 0.15 eq, 0.051 mmol), K_3PO_4 (288.90 mg, 4.0 eq, 1.361 mmol) in 5 mL anhydrous toluene and stirred in 105°C for 5 hours and 1 mL degassed DI was added. Polymerized using thermal reactor (reaction condition: 105 °C 7 days) under Ar. Then, the polymer was end cap using and bromobenzene and phenylboronic acid. Polymer mixture was cooled to room temperature, and the viscous mixture was poured into methanol (≈ 400 mL). After stirring for 1h, the precipitated solid was collected by gravity filtration. The crude polymer solid was subjected to sequential Soxhlet extractions with methanol, acetone, hexane, and chloroform. Finally, the concentrated chloroform solution (≈ 1 mL) was precipitated into methanol (≈ 200 mL). The final precipitate was collected by vacuum filtration and dried under reduced pressure to give the pure polymer as an brown solid.

2. Experimental section

Polymer characterization*:* ^{1}H-Nuclear magnetic resonance (NMR) (500 MHz) spectra were recorded on a Bruker AVANCE III HD 500-MHz NMR spectrometer in $CDCl_3$. Thermo gravimetric analysis (TGA) was performed using Thermo plus EVOII TG8120; the samples were run under N_2 and heated from room temperature to 500 °C at a rate of 10 °C/min. UV-vis absorption measurements were performed with a double-beam Shimadzu UV-2550 spectrophotometer over 400–800 nm. All solutions used in the UV-vis experiments were run in chloroform. Metal contents were determined by inductively coupled plasma (ICP) spectroscopy on polymer samples. Pd contents were determined by ICP-MS (PerkinElmer ICP MS NexION 2000).

Preparation of the polymer nanoparticle*:* The conjugated polymer nanoparticles were synthesized via a nanoprecipitation method. Initially, 2 mL of an conjugtaed polymer solution in THF (1 mg mL^{-1}) was blended with 2 mL of PS-PEG-COOH in THF (4 mg mL^{-1}) and sonicated for 5 min to ensure a homogeneous mixture. This organic phase was then rapidly injected into 12 mL of distilled water under continuous sonication. Subsequent evaporation of the THF was carried out in an ambient air hood over 3~4 days. To remove large aggregations, the dispersion was filtered with a 0.4 μm PVDF syringe filter.

***Photocatalytic H_2 evolution**:* Measurements were conducted in a 50 mL quartz flask. Catalysts (normally 1 mg for polymer stock) were dispersed into 0.6 M ascorbic acid (with buffer NaOH 2.5 M) water solution (50 mL). After bubbling with Ar for 30 min to remove O_2, the reaction mixture was illuminated with a 300 W Newport Xe light source (Model: 66160, Ozone free) using a 420 nm cut-off filter. The lightsource was cooled by water circulating through a metal jacket. Gas samples were taken out by using agas-tight syringe and run on a Nexis GC-2030 gas chromatograph. Hydrogen was detected with a thermal conductivity detector referencing against standard gas with a known concentration of hydrogen. Any hydrogen dissolved in the reaction mixture was not measured and the pressure increase generated by the evolved hydrogen was neglected in the calculations.

***Particle morphology analysis**:* Nanoparticle tracking analysis (NTA) was performed using a ZetaView® particle analyzer (Particle Metrix GmbH, Germany) equipped with a 488 nm laser. Prior to each measurement, the system was thoroughly rinsed with deionized (DI) water and calibrated using a 100 nm polystyrene standard bead suspension, following the manufacturer's protocol. Samples were prepared in an aqueous solution and diluted to a suitable concentration ensure an optimal particle count (green) per frame. A 1 mL syringe was used to inject the diluted sample into the sample cell, taking care to avoid air bubbles. For each sample, at least five measurements were conducted at 11 different positions within the sample cell to ensure a statistically robust analysis.

Hydrogen evolution rate (HER) measurement: Measurements were conducted in a 50 mL quartz flask. Conjugated polymer photocatalysts nanoparticles were dispersed into ascorbic acid solutions 50 mL (0.2 M Ascorbic Acid pH 4, buffer with NaOH). After purging with Ar for 20 min to remove O_2, the reaction mixture was illuminated with a 300-W Newport Xe light-source (Model: 66160, Ozone free) using a AM 1.5G filter. Hydrogen was detected with a thermal conductivity detector by comparison with a standard gas with a known concentration of hydrogen and analyzed on a Nexis GC-2030 gas chromatograph. Any hydrogen dissolved in the reaction mixture was not measured, and the pressure increase generated by the evolved hydrogen was neglected in the calculations. We used about 0.95 mg for the photocatalytic activity. The performance of the photocatalysts and its concentration are proportional up to a certain threshold, beyond which it reaches a saturated state due to reflection, scattering and so

on. For these reasons, we use this concentration for higher absorbance under photocatalytic conditions.

***Apparent quantum yield (AQY) measurement**:* Apparent quantum yield (AQY) was determined under the conditions used for photocatalytic hydrogen generation experiments in a 3.5 mL airtight quartz cuvette (path length 1 cm). The solution was illuminated by a 300 W Newport Xe light-source (Model: 66160, Ozone free) as a light source equipped with an 420 nm cutoff filter and monochromated with a bandpass filter to 420, 450, 500, and 550 nm. And AQY were calculated from following equation:

$$AQY(\%) = 2 \times \frac{moles\ of\ hydrogen}{moles\ of\ incident\ lights} = 2 \times \frac{M \times N_A \times h \times c}{A \times P \times t \times \lambda} \times 100\% \qquad (1)$$

where M is the production of H_2 (mol sec^{-1}); N_A is Avogadro's constant 6.02×10^{23} mol^{-1}; h is Planck's constant 6.62×10^{-34} J·s; c is the light speed under vacuum 3.00×10^{8} m s^{-1}; A is the area of light irradiation; λ is the light wavelength; P is the incident monochromatic light intensity at λ; and t is the irradiation time at λ.

Photophysics analysis: Time-resolved photoluminescence (TR-PL) data were measured by the time-correlated single-photon-counting (TCSPC) method (Edinburgh Instruments Ltd, FS5 Spectrofluorometer) with an excitation wavelength of 540 nm. Nanosecond – microsecond transient absorption spectroscopy (ns-μs TAS) data were collected using a pump – probe TA spectroscopy, which consisted of a TA spectrometer and a regenerative amplified Nd:YAG laser (EL-YAG) with a pulse width of 6-8 ns. The pulse is capable of generating both visible pulses (532 nm) and UV pulses (355 nm) through a third harmonic generator. The TA spectra data were collected over a time range from 6 ns to 500 ns. The probe beam is derived from a 150 W Xenon lamp, which is reflected off the nanoparticle sample and then passed through a monochromator before reaching a PMT-980 photodiode detector. To simultaneously capture data on two different time scales, the comprehensive L900 spectrometer software (V9.4.3) package is utilized, and the nanosecond-microsecond signal is sampled using an oscilloscope (Tektronix MDO30232, Beaverton, OR, USA). Excitation fluences are measured using a pyroelectric energy sensor.

Liquid-Phase Transmission Electron Microscopy (LP-TEM): To observe the nanoparticles in their native solvated state, LP-TEM analysis was conducted utilizing graphene liquid cells (GLCs) prepared via a literature method. Graphene-coated grids were obtained through the direct transfer of graphene from Cu foils. The sample was prepared by sandwiching a small aliquot of the nanoparticle solution between two graphene-coated grids; the excess liquid was carefully removed by clamping to ensure the formation of a thin liquid layer encapsulated by graphene. Imaging was carried out on a Tecnai G2 F20 TWIN TMP system (FEI, Thermo Fisher Scientific) at 200 kV, allowing for high-resolution observation of the polymer nanostructures without drying-induced artifacts

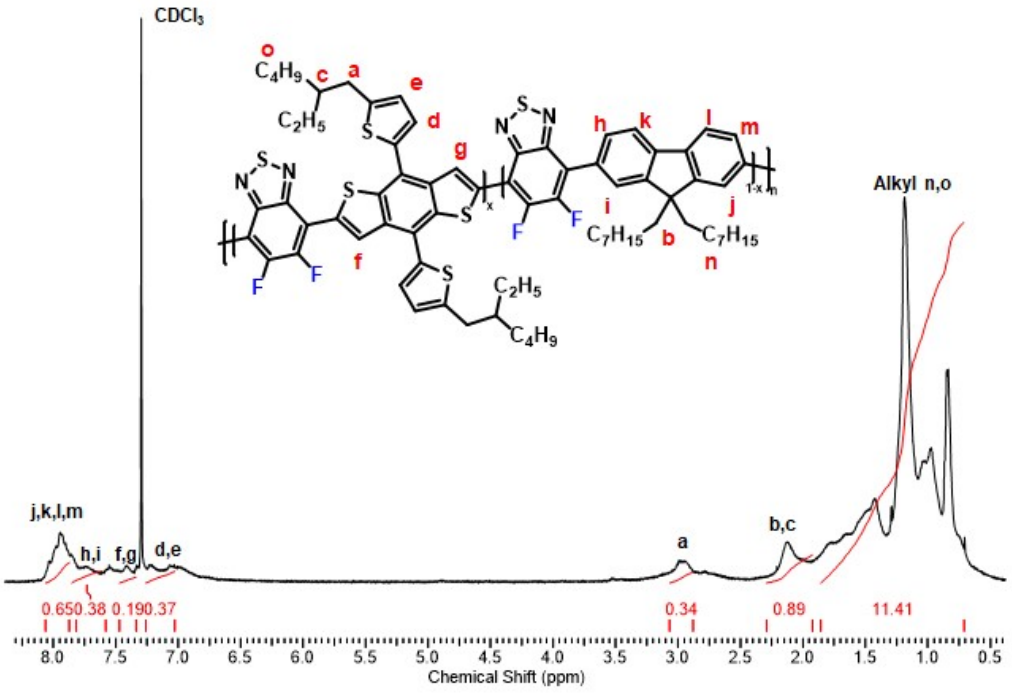

Figure S1. ^{1}H-NMR spectrum of PBF8BT-AF.

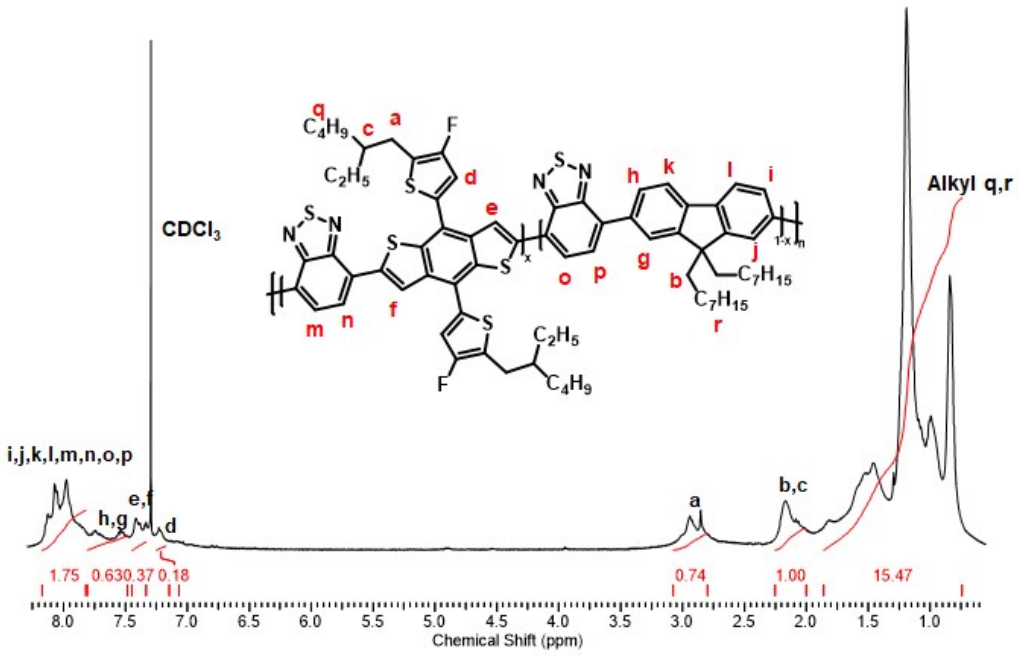

Figure S2. ^{1}H-NMR spectrum of PBF8BT-DF.

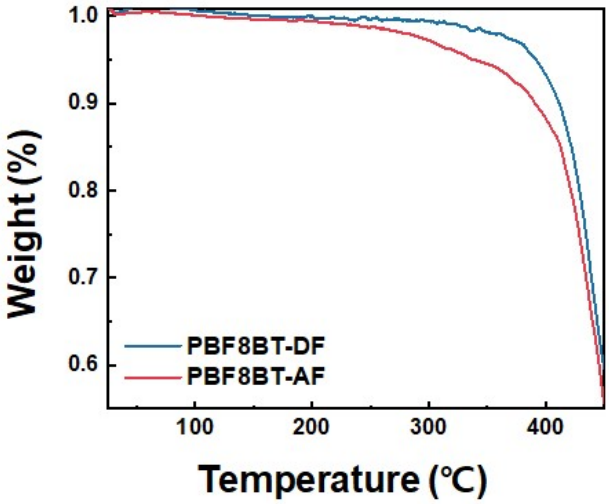

Figure S3. Thermal gravimetric analysis (TGA) profile of PBF8BT-AF and PBF8BT-DF.

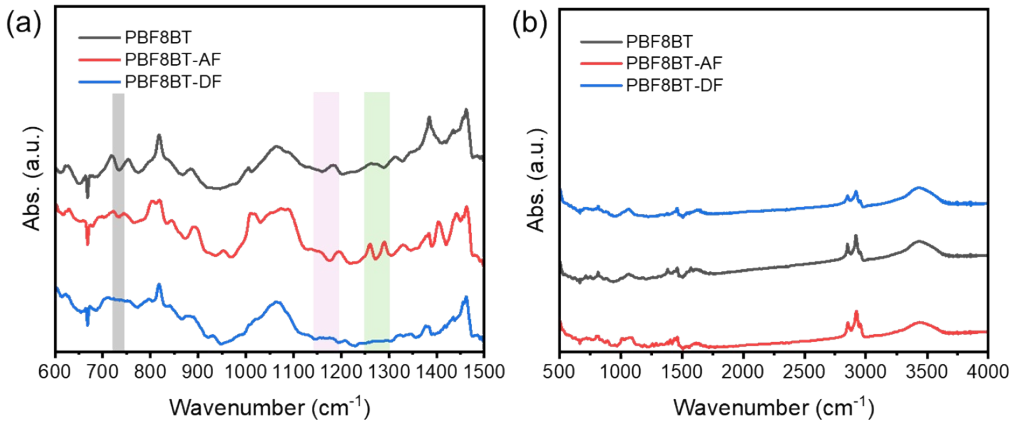

Figure S4. Full-range FT-IR absorption spectra of the polymer series: PBF8BT (black line, non-fluorinated), PBF8BT-AF (red line, mono-fluorinated), and PBF8BT-DF (blue line, di-fluorinated), all prepared using the KBr pellet method for high-fidelity signal detection. (a) Enlarged spectra in the 600–1500 cm^{-1} fingerprint region and (b) full spectra in the 500–4000 cm^{-1} range for PBF8BT (black), PBF8BT-AF (red), and PBF8BT-DF (blue). In panel (a), the highlighted regions correspond to: 720–740 cm^{-1} (grey box), 1150–1200 cm^{-1} (pink box), and 1250–1300 cm^{-1} (green box), which are discussed in relation to aromatic C–H out-of-plane bending and C–F-related vibrational features.

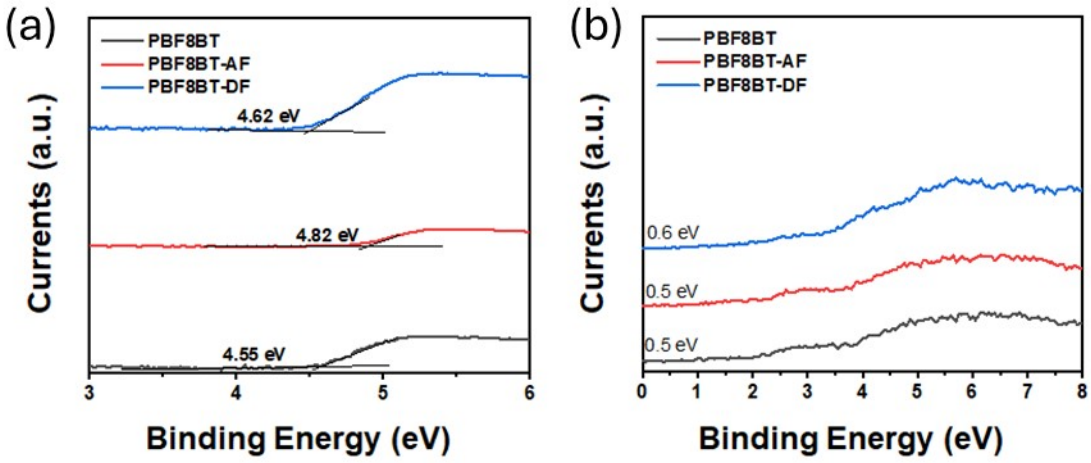

Figure S5. (a) Ultraviolet photoelectron spectroscopy (UPS) spectra of PBF8BT, PBF8BT-AF, and PBF8BT-DF films showing the HOMO energy levels. (b) Corresponding valence band region used to determine the onset energies.

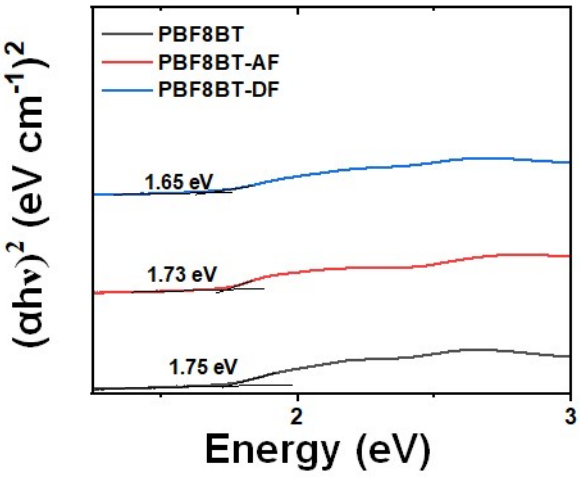

Figure S6. Tauc plot profile of PBF8BT-x polymers.

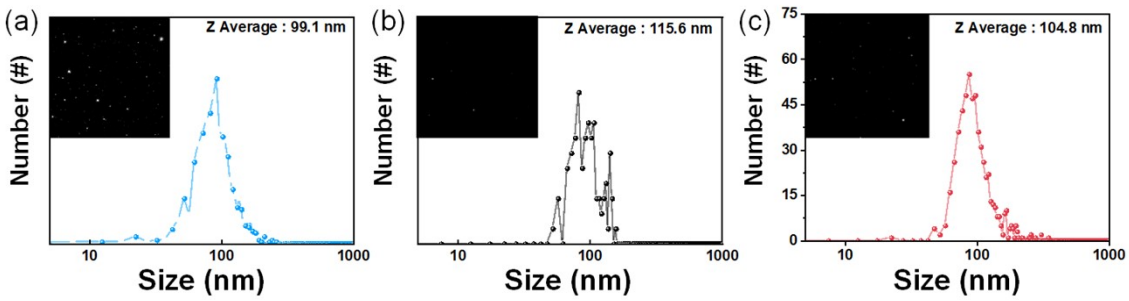

Figure S7. Nanoparticle tracking analysis (ZetaView® x30) of (a) PBF8BT, (b) PBF8BT-AF, and (c) PBF8BT-DF nanoparticles dispersed in water.

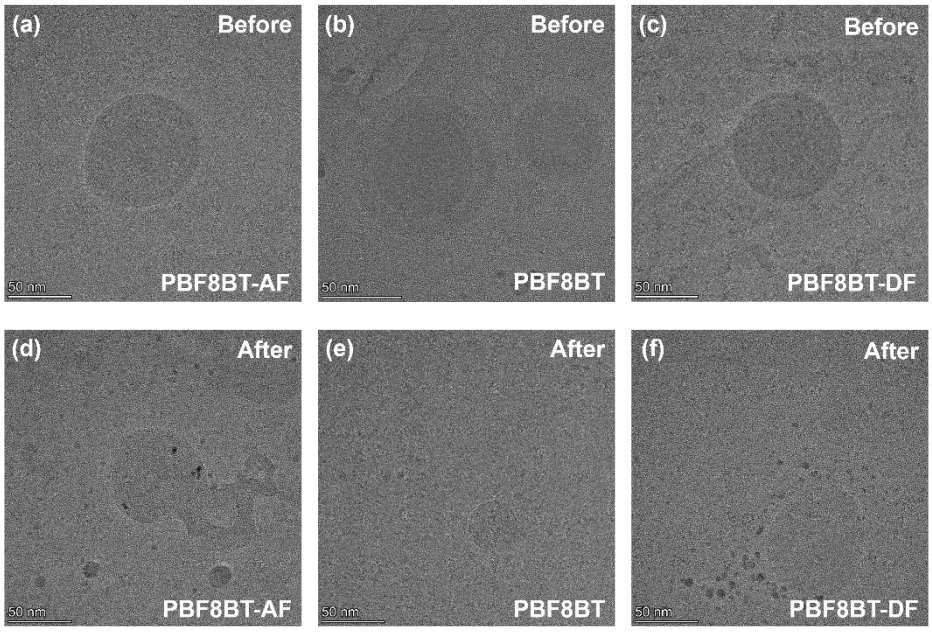

Figure S8. LP-TEM images of the Pdots before and after photocatalysis. As-prepared (a) PBF8BT-AF, (b) PBF8BT, and (c) PBF8BT-DF. Corresponding images of (d) PBF8BT-AF, (e) PBF8BT, and (f) PBF8BT-DF after the photocatalytic hydrogen evolution reaction (conducted with Pt cocatalyst and 0.2 M ascorbic acid). The images demonstrate that the spherical morphology and size distribution of the Pdots remain unchanged post-reaction, confirming their excellent structural integrity.

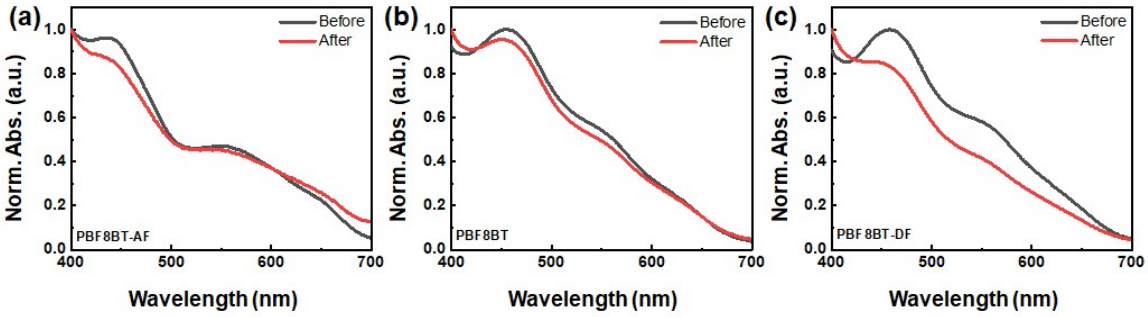

Figure S9. UV-Vis absorption spectra of (a) PBF8BT-AF, (b) PBF8BT, and (c) PBF8BT-DF before and after the photocatalytic stability tests. In each plot, the black and red lines represent the spectra before irradiation and after light irradiation, respectively. The overlapping spectral profiles demonstrate the high structural and electronic stability of the Pdots during the photocatalytic process.

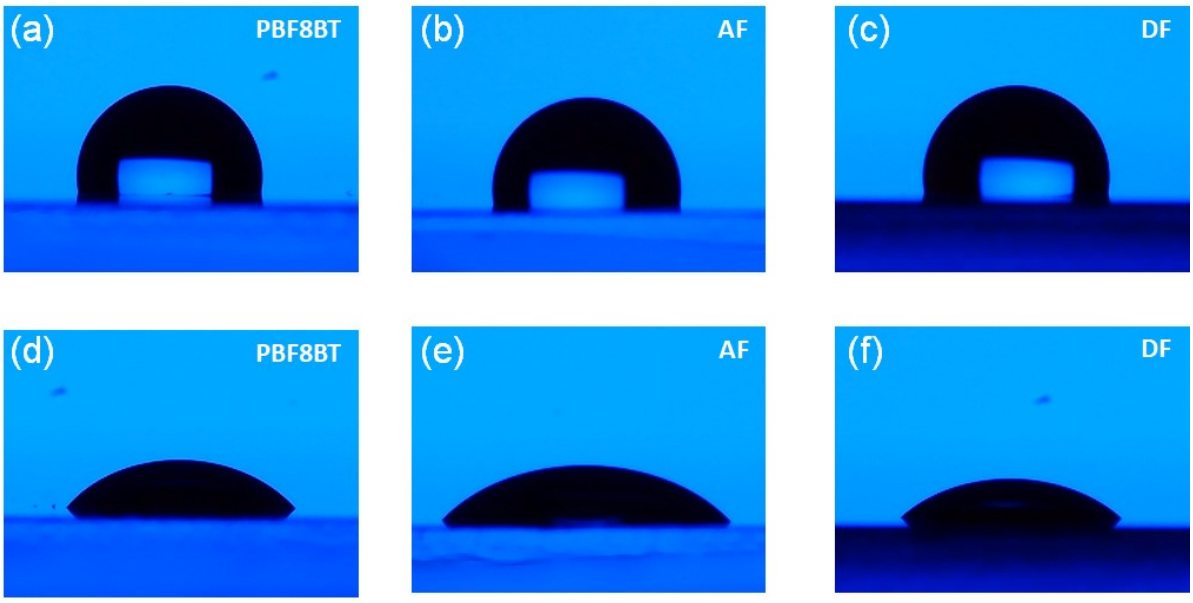

Figure S10. Contact angle measurements of polymer thin films. (a–c) Water contact angles of PBF8BT, PBF8BT-AF, and PBF8BT-DF, recorded as 98.93°, 95.69°, and 96.56°, respectively. (d–f) Diiodomethane contact angles of PBF8BT, PBF8BT-AF, and PBF8BT-DF, recorded as 44.72°, 47.75°, and 44.52°, respectively. The corresponding surface energies derived from the water contact angles were 48.09, 44.21, and 46.44 mN m^{-1} for PBF8BT, PBF8BT-AF, and PBF8BT-DF, respectively. The surface energy of polymer thin films was calculated using the Owens–Wendt–Rabel–Kaelble (OWRK) method.

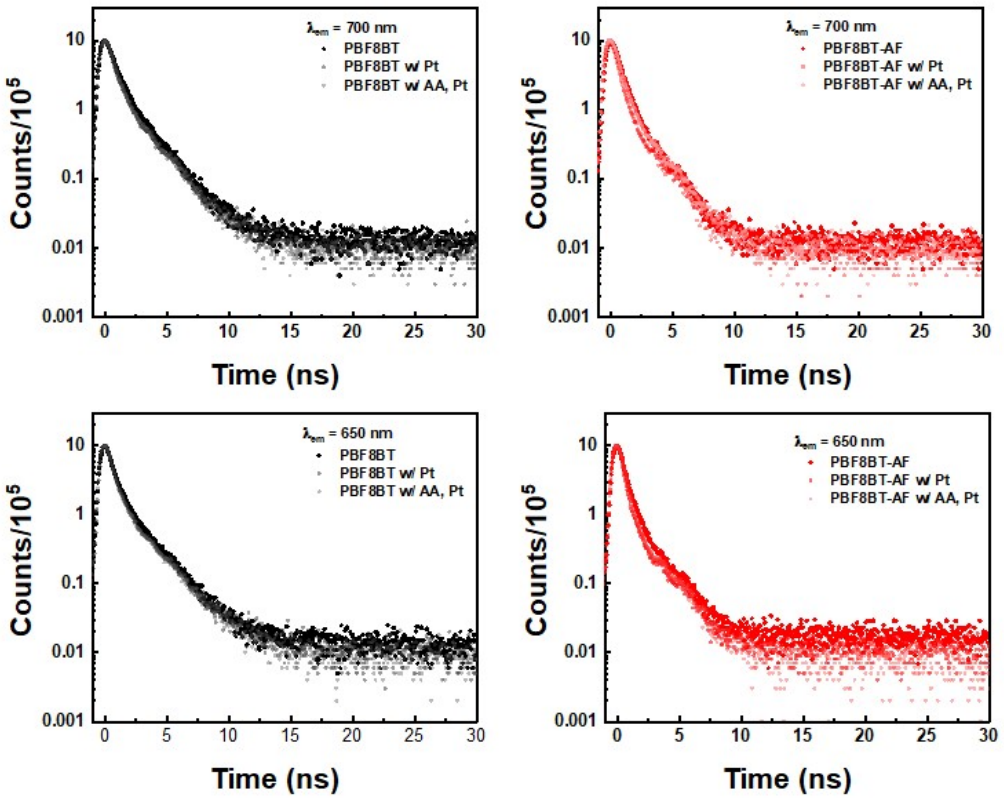

Figure S11. Time-resolved photoluminescence (TR-PL) decay profiles of PBF8BT and PBF8BT-AF Pdots measured by time-correlated single photon counting (TCSPC). (a, c) TR-PL decays of PBF8BT Pdots monitored at 700 and 650 nm, respectively, under three conditions: without Pt cocatalyst, with Pt cocatalyst, and with Pt cocatalyst plus ascorbic acid (AA). (b, d) Corresponding TR-PL decays of PBF8BT-AF Pdots under the same conditions.

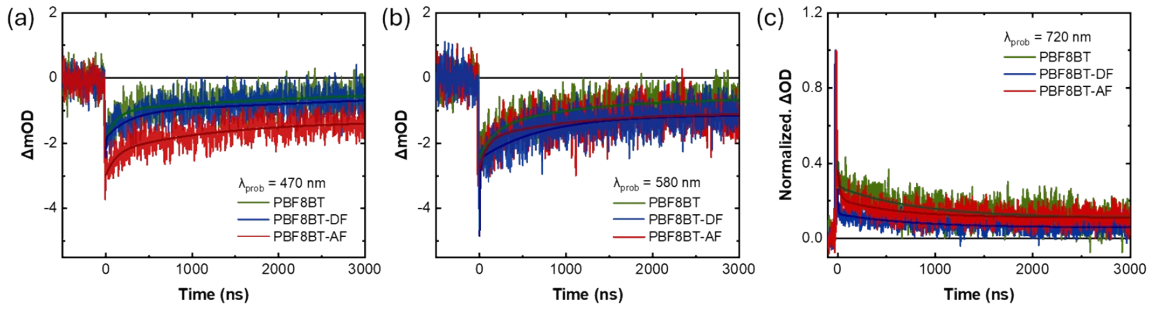

Figure S12. Transient absorption kinetics of nanoparticles based on PBF8BT (green), PBF8BT-DF (blue), and PBF8BT-AF (red) probed at (a) 470 nm, (b) 580 nm, and (c) 720 nm.

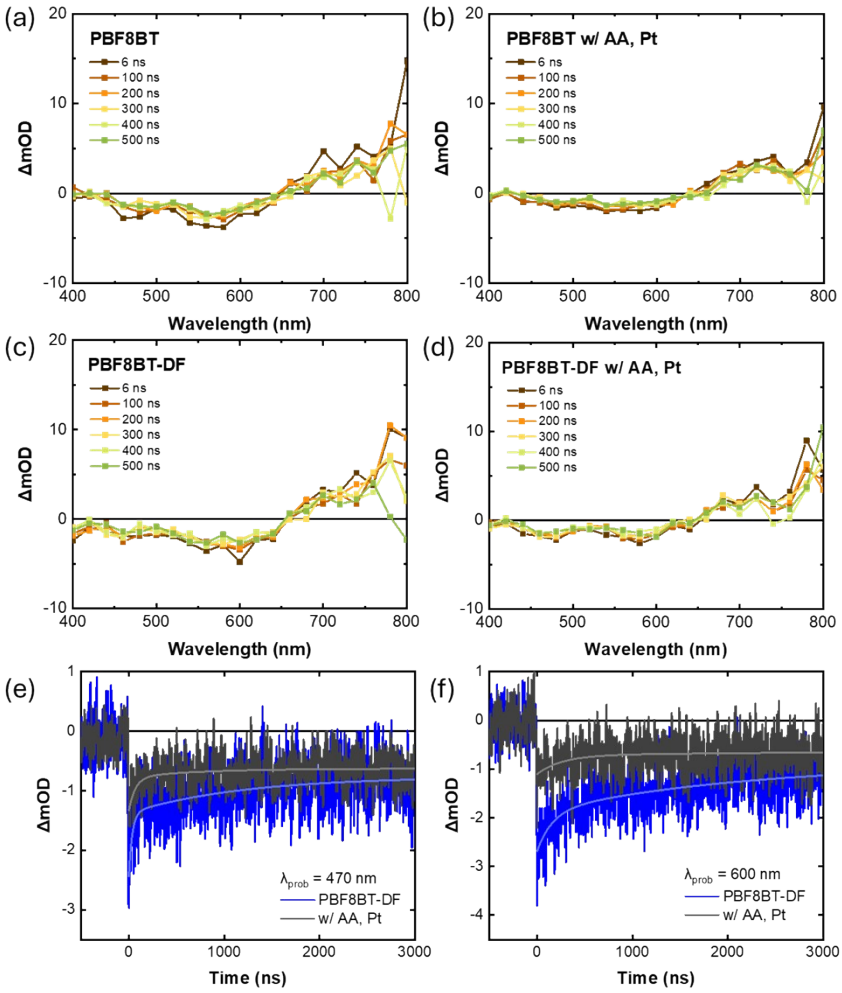

Figure S13. Transient absorption spectroscopy of nanoparticles under photocatalytic conditions. TAS spectra of (a-b) PBF8BT and (c-d) PBF8BT-DF measured in the absence (left) and presence (right) of ascorbic acid (AA) and Pt cocatalyst. TAS kinetics of PBF8BT-DF at probe wavelengths of (e) 470 nm and (f) 600 nm, comparing the relaxation behaviors with and without AA and Pt.

Table S1. Thermal, optical, and electrochemical properties of the PBF8BT.

Polymers	M_n [kg mol^{-1}][a)]	PDI	T_d [°C][b)]	λ_{max} [nm]	λ_{edge} [nm]	E_g^{opt} [eV][c)]	LUMO [eV][d)]	HOMO [eV][e)]
PBF8BT	12.7 k	2.41	379	451	640	1.75	-3.30	-5.05

[a] Determined by gel permeation chromatography (GPC) using tetrahydrofuran as an eluent at 40°C, relative to a polystyrene standard.
[b] Thermal decomposition temperature (5% weight loss) determined by TGA under N_2.
[c] Optical band gap estimated from the absorption edges (λ_{edge}) in the solution state.
[d] Lowest unoccupied molecular orbital (LUMO) levels were estimated from the onset of the first reduction potentials with reference to ferrocene at -4.8 eV.
[e] HOMO = LUMO + E_g^{opt}.

Table S2. Summary of residual palladium (Pd) in synthesized polymers, PBF8BT, PBF8BT-AF, and PBF8BT-DF, respectively.

	Pd concentration [%]
PBF8BT	0.28
PBF8BT-AF	0.14
PBF8BT-DF	0.19

Table S3. Time-resolved photoluminescence (TR-PL) decay lifetime of PBF8BT series excited at 450 nm and probed at 680 nm. The decay kinetics were fitted using a bi-exponential function: $I(t) = A_1 \exp(-t/\tau_1) + A_2 \exp(-t/\tau_2)$.

	A_1	τ_1 (=ns)	A_2	τ_2 (=ns]
PBF8BT	9447	0.73	1319	2.91
PBF8BT-AF	10411	0.66	400.2	3.60
PBF8BT-DF	9286	0.56	1324	2.62

Table S4. TR-PL decay lifetime of PBF8BT-DF with various conditions, without Pt, with Pt, or with AA and Pt excited at 450 nm and probed at 700 nm. The decay kinetics were fitted using a bi-exponential function: $I(t) = A_1 \exp(-t/\tau_1) + A_2 \exp(-t/\tau_2)$.

	A_1	τ_1 (=ns)	A_2	τ_2 (=ns)
PBF8BT-DF	10791	0.87	442.06	4.51
PBF8BT-DF w/ Pt	11229	0.68	161.61	7.05
PBF8BT-DF w/ AA, Pt	10827	0.65	269.17	4.97

Table S5. Kinetic parameters derived from the ns-TA decay kinetics of fluorinated polymer Pdots (PBF8BT-AF and PBF8BT-DF). Comparison of the decay lifetimes (τ_1 and τ_2) and their corresponding amplitudes (A_1 and A_2) at 470 nm and 580 nm. The decay kinetics were fitted using a bi-exponential function: $I(t) = A_1 \exp(-t/\tau_1) + A_2 \exp(-t/\tau_2)$.

Probed wavelength	Materials	A_1	τ_1 (=ns)	A_2	τ_2 (=ns)
470 nm	PBF8BT-AF	-0.00070	114.08	-0.00098	1307
	PBF8BT-DF	-0.00085	256.78	-	-
580 nm	PBF8BT-AF	-0.00089	88.41	-0.00080	1057
	PBF8BT-DF	-0.0023	8.24	-0.001	728.98

Table S6. Kinetic parameters derived from the ns-TA decay kinetics of fluorinated polymer Pdots (PBF8BT, PBF8BT-AF and PBF8BT-DF). Comparison of the decay lifetimes (τ_1 and τ_2) and their corresponding amplitudes (A_1 and A_2) at 720 nm. The decay kinetics were fitted using a bi-exponential function: $I(t) = A_1 \exp(-t/\tau_1) + A_2 \exp(-t/\tau_2)$.

Materials	A_1	τ_1 (=ns)	A_2	τ_2 (=ns)	τ_{avg} (=ns)
PBF8BT	0.13	10.2	0.16	813	1001
PBF8BT-AF	0.14	22.7	0.09	597	396.1
PBF8BT-DF	0.10	5.53	0.07	781	536.1

Table S7. Bi-exponential fitting parameters extracted from transient absorption (TA) decay kinetics of PBF8BT-DF monitored at 470 and 600 nm under operative conditions (with Pt cocatalyst and ascorbic acid (AA)). Comparison of the decay lifetimes (τ_1 and τ_2) and their corresponding amplitudes (A_1 and A_2). The decay kinetics were fitted using a bi-exponential function: $I(t) = A_1 \exp(-t/\tau_1) + A_2 \exp(-t/\tau_2)$.

Probed wavelength	Materials	A_1	τ_1 (=ns)	A_2	τ_2 (=ns)
470 nm	PBF8BT-DF	-0.001	35.05	-0.0006	1190
	PBF8BT-DF, w/ Pt, AA	-0.0005	69.05	-0.0014	725.1
600 nm	PBF8BT-DF	-0.0007	157.9	-0.001	2124
	PBF8BT-DF, w/ Pt, AA	-0.0003	263.4	-	-